Kinetics and Products of the IO Self-Reaction

William J. Bloss,[†] David M. Rowley,[‡] R. Anthony Cox,* and Roderic L. Jones

Centre for Atmospheric Science, University Chemical Laboratories, University of Cambridge, Lensfield Road, Cambridge, CB2 1EW, U.K.

Received: December 14, 2000

The absorption cross sections of the gas-phase IO radical and the kinetics and products of the IO self-reaction have been measured using the technique of laser photolysis with time-resolved UV−vis absorption spectroscopy. The IO absorption cross section at the peak of the (4,0) vibronic band of the ($A^2\Pi \leftarrow X\ ^2\Pi$) transition at 427.2 nm, determined using the reaction $O(^3P) + CF_3I$ to form IO and calibrated relative to the O_3 cross section was found to be $(1.9 \pm 0.17) \times 10^{-17}$ cm^{2}molecule^{-1} at 295 K and 1.13 nm fwhm spectral resolution. The IO cross sections were found to exhibit a negative temperature dependence. The kinetics of the IO self-reaction were measured using the reaction $O(^3P) + I_2$ to form IO, and the self-reaction rate coefficient k_1, determined from the loss of IO radicals in the absence of ozone, was found to be $(8.2 \pm 1.3) \times 10^{-11}$ molecules^{-1} cm^3 s^{-1} at 295 K and 760 Torr. The self-reaction rate coefficient was found to be independent of pressure between 100 and 760 Torr, and to display a negative temperature dependence between 222 and 325 K, described by $k_1 = (4.1 \pm 3.4) \times 10^{-11} \exp\{(220 \pm 230)/T\}$ molecules^{-1} cm^3 s^{-1}. All errors are 2σ. Four potential product channels exist for the IO self-reaction: IO + IO → 2I + O_2 (1a), IO + IO → I_2 + O_2 (1b), IO + IO → OIO + I (1c), IO + IO + M → I_2O_2 + M (1d). No direct measurement of I atom production was performed. I_2 formation was observed, but attributed to IO-catalyzed I atom recombination (I + IO + M → I_2O + M; I + I_2O → I_2 + IO). OIO formation was observed and shown to result from the IO self-reaction. Formation of a broadband absorbing product underlying the IO absorption at low ($\lambda < 400$ nm) wavelengths was observed, and tentatively attributed to I_2O_2. The OIO cross sections and yield from the IO + IO reaction were determined via measurement of OIO production from the IO + BrO reaction which allowed limits to be placed on the branching ratio for OIO formation in the IO self-reaction at 295 K and 760 Torr. Branching ratios for all reaction channels were found to lie in the ranges $0.07 \leq k_{1a}/k_1 \leq 0.15$, $k_{1b}/k_1 \leq 0.05$, $0.30 \leq k_{1c}/k_1 \leq 0.46$, and $0.42 \leq k_{1d}/k_1 \leq 0.55$ at 295 K and 760 Torr. The results are compared with previous studies of the IO self-reaction, and their implications for atmospheric iodine chemistry are considered.

1. Introduction

Gas phase halogen monoxide radicals play a key role in catalytic cycles which can destroy atmospheric ozone.[1] Consequently, reactions of these species have been the subject of numerous kinetic and mechanistic studies in recent years.[2] The importance of chlorine and bromine species in atmospheric chemistry is now widely recognized, and current models of atmospheric composition and chemistry incorporate an extensive database of chlorine and bromine reactions,[3] In contrast, the role of iodine in the atmosphere is less well-known but, following trends of reactivity through the halogens, potentially significant. This work, and that in the accompanying paper, investigates the gas-phase chemistry of a key species in the atmospheric chemistry of iodine: the IO radical.

IO is formed in the atmosphere following the photooxidation of iodine containing source gases. The principal sources of iodine-containing species emitted to the atmosphere are organic, and are believed to be of biogenic origin, produced by marine organisms.[4] The most abundant iodocarbon in the atmosphere is CH_3I, with observed atmospheric concentrations typically ranging from 1 to 3 pptv,[5,6] with higher concentrations, up to 43 pptv, reported in regions of high biological productivity.[7] Other alkyl iodide species (e.g., CH_2I_2, C_2H_5I, and CH_2IBr) have also been detected in the atmosphere, and may even dominate iodine emissions in some marine locations.[8] Direct anthropogenic sources of atmospheric iodine, principally CF_3I, are estimated to account for less than 10% of the total iodine source, although release of iodine through biomass burning also contributes to the atmospheric iodine budget.[9] The biogenic iodocarbons are all photolabile in the atmosphere, with lifetimes with respect to solar photolysis ranging from minutes[10] (CH_2I_2) to a few days[11] (CH_3I). Solar photolysis of iodocarbons (RI) releases iodine atoms which react with atmospheric ozone producing IO radicals:

$$RI + h\nu \rightarrow R + I \quad (2)$$

$$I + O_3 \rightarrow IO + O_2 \quad (3)$$

The principal fates of the IO radical in the atmosphere are solar photolysis (reaction 4) and gas-phase reaction with other atmospheric constituents.

$$IO + h\nu \rightarrow I + O(^3P) \quad (4)$$

* To whom correspondence should be addressed. E-mail: rac26@cam.ac.uk. FAX: + 44 1223 336362.

[†] Present address: Jet Propulsion Laboratory, California Institute of Technology, Pasadena, CA 91109. E-mail: wbloss@jpl.nasa.gov.

[‡] Present address: University College London, Chemistry Department, Christopher Ingold Laboratories, 20 Gordon Street, London WC1H 0AJ, UK. E-mail: d.m.rowley@ucl.ac.uk.

10.1021/jp0044936 CCC: $20.00
Published on Web 07/31/2001

The atmospheric role of IO is thus determined by its photolysis rate, and the nature and rates of the reactions of IO with other trace species, e.g. HO_2, NO_2, ClO, BrO, and IO. Solar photolysis of IO in the atmosphere is followed by reformation of IO via reaction 3, consuming ozone. This is offset by reaction of the oxygen atom coproduced in reaction 4 with atmospheric oxygen reforming ozone, thus IO photolysis is a null cycle with respect to ozone loss. In contrast, reactions that convert IO to I, either directly or indirectly, without concomitant regeneration of odd-oxygen, can lead to catalytic ozone loss. For example, the reaction of IO with HO_2 followed by the photolysis of HOI completes a catalytic cycle for ozone loss:[12]

$$IO + HO_2 \rightarrow HOI + O_2 \quad (5)$$

$$HOI + h\nu \rightarrow OH + I \quad (6)$$

$$I + O_3 \rightarrow IO + O_2 \quad (3)$$

$$\text{net:} \quad HO_2 + O_3 \rightarrow OH + 2O_2$$

Several similar cycles can occur involving reactions of IO with other species (e.g. IO, ClO, BrO, etc.) In competition with such cycles, iodine can form "reservoir species" (e.g. HI, $IONO_2$) which sequester "active" iodine (I and IO) and mitigate ozone loss. However, iodine reservoirs are formed less readily than their chlorine and bromine counterparts. For example, formation of HI by hydrogen abstraction is only possible in the atmosphere in the reaction of I with HO_2,[13] whereas Cl, and to a lesser extent Br, can abstract hydrogen from many organic species.[14] Iodine reservoir species are also less thermally and photolytically stable than their chlorine and bromine analogues. Because iodine reservoirs are formed only slowly and are unstable, the fraction of total inorganic iodine present in active forms is much greater than the equivalent fractions for chlorine and bromine, and even a small abundance of iodine has the potential to make a significant impact upon atmospheric ozone levels.[9]

The potential for iodine chemistry to contribute to the destruction of ozone in the troposphere has been considered by Davis et al.[6] They calculated that iodine chemistry could account for between 6 and 30% of the total column ozone destruction rate in the troposphere, for inorganic iodine mixing ratios of 1.5 and 7 pptv, respectively. Davis et al. also showed that iodine chemistry can perturb the concentrations and ratios of other trace species, e.g., [OH]/[HO_2] and [NO]/[NO_2]. On the basis of their measurements of CH_3I over the Pacific Ocean, Davis et al. suggested that the lower total iodine (1.5 pptv) scenario was in general more representative of the marine troposphere, but also pointed out the considerable potential for iodine to have a significant impact on tropospheric ozone levels in regions of high source activity, such as those discussed above.

The IO radical has recently been observed in the troposphere, in the course of DOAS observations in the marine boundary layer (MBL).[15,16] IO was detected at concentrations of up to 9 pptv, with associated observations of the alkyl iodide species CH_2I_2, C_2H_5I, and CH_3I.[8] Modeling studies based upon these observations show that the IO self-reaction is a major gas-phase reaction process for IO, and have confirmed that iodine chemistry can lead to significant MBL ozone destruction.[16−18]

The possibility that iodine might also play a role in stratospheric chemistry was initially raised by Solomon et al.[9] These authors showed, in a modeling study, that lower stratospheric total iodine abundances of 1 pptv would have a profound impact on ozone concentrations, provided that the gas-phase reactions of the IO radical were rapid and produced I atoms. Because of the short lifetime of surface-emitted iodine source gases[10] stratospheric abundances of iodine of 1 pptv would require rapid vertical transport of air to the stratosphere, and the first measurements[19,20] of stratospheric composition aimed at detecting iodine suggested that this amount was unlikely to be present. Wennberg et al.[19] placed an upper limit of 0.2 $\binom{+0.2}{-0.3}$ pptv on the total inorganic iodine abundance in the lower stratosphere at mid-latitudes. Similarly, Pundt et al.[20] derived a limit of 0.2 pptv of IO in the stratosphere at high latitudes. Very recently, however, Wittrock et al.[21] have reported a definitive observation of stratospheric IO, above Spitzbergen. In a series of observations made since 1995, stratospheric IO was detected each year, with a polar stratospheric IO mixing ratio of in the range 0.65−0.80 pptv (± 0.2 pptv) in Spring 1997. These results imply that iodine can indeed play a significant role in the stratosphere, dependent upon the nature and rates of the gas-phase reactions of IO.

TABLE 1: Comparison of Determinations of the IO Absorption Cross Section at 427.2 nm (Peak of the (4,0) Band) at 295−303 K

authors	date	σ(IO) × 10^{17}, molecule^{-1} cm^2	fwhm resolution, nm
Cox and Coker[24]	1983	$3.1^{+2}_{-1.5}$	0.27
Jenkin and Cox[25]	1985	2.2 ± 0.5	0.27
Sander[26]	1986	3.1 ± 0.3	0.17
Stickel et al.[27]	1988	3.1 ± 0.6	0.3
Laszlo et al.[28]	1995	2.8 ± 0.5	0.3
Harwood et al.[29]	1997	3.0 ± 0.4	0.44
Harwood et al.[29]	1997	3.6 ± 0.5	0.14
Harwood et al.[29]	1997	2.3 ± 0.3	0.44 smoothed to 1.13
this work		1.9 ± 0.2	1.13

Quantification of the role of iodine chemistry in the atmosphere requires measurement of the absorption cross sections of IO, both to determine its atmospheric photolysis rate and to permit detection of IO via absorption spectroscopy, in both the laboratory and the field. A knowledge of the kinetics and products of the IO self-reaction is also required, to determine the importance of this reaction in the troposphere and to conduct laboratory studies of other aspects of the chemistry of IO. To this end, several studies of the kinetics and photochemistry of gas-phase iodine species have been reported in the literature.

Previous studies of the UV−vis absorption spectrum of IO (σ_{IO})[22−29] all show that the UV absorption, arising from the ($A^2\Pi \leftarrow X^2\Pi$) electronic transition, consists of a continuum shoulder between 340 and 400 nm with vibronic structure to higher wavelengths, extending to approximately 470 nm. Reported absorption cross sections of IO across the resolution-independent shoulder show reasonable agreement, but comparison of the cross sections measured in the structured region is complicated by the dependence of σ_{IO} on instrumental resolution. Reported measurements of the IO absorption cross sections at the (4,0) band head are compared in Table 1. The temperature dependence of σ_{IO} at the (4,0) band head has been studied by Sander[26] and by Harwood et al.[29] These studies are not in agreement: Sander observed a pronounced negative temperature dependence to σ_{IO} between 250 and 373 K, whereas Harwood et al. report a temperature-independent σ_{IO} between 203 and 373 K.

The kinetics and products of the IO self-reaction have been the subject of several studies, employing discharge-flow/absorption spectroscopy,[23] modulated-photolysis/absorption spectroscopy,[24,25,30,31] discharge-flow/mass spectrometry,[32,33] pulsed-photolysis/absorption spectroscopy[26−29,34] and discharge-flow/resonance fluorescence. Comparison of the results obtained is complicated by the use of different chemical systems and, in

TABLE 2: Comparison of Determinations of the IO Self-Reaction Rate Coefficient at 295−298 K, Measured in Non-Ozone Systems

study	year	experimental technique[a]	chemical system	$k \times 10^{11}$/molecules^{-1} cm^3 s^{-1}	pressure/Torr
Sander[26]	1986	FP/UVA	O + I_2	5.5 ± 1.1	50−700
Martin et al.[32]	1987	DF/MS	O + I_2	3 ± 0.5	1
Barnes et al.[32]	1991	DF/MS	O + I_2	5.5 ± 0.8	1−5
Laszlo et al.[28]	1995	LFP/UVA	O + I_2	8.0 ± 1.8	60−610
Harwood et al.[29]	1997	LFP/UVA	O + I_2	10.1 ± 0.4	610
Atkinson et al.[34]	1999	LFP/CRDS	O + CF_3I	10 ± 3	9.4, 30.1
Vipond[35]	1998	DF/LIF	O + CF_3I	9.3 ± 1.0	2−4
Ingham et al.[31]	2000	LFP/UVA	O + I_2	9.0 ± 1.7	60
this work		LFP/UVA	O + I_2	8.2 ± 1.0	100−760

[a] FP = flash photolysis, LFP = laser flash photolysis, DF = disharge flow, UVA = UV−vis absorption spectroscopy, LAS = laser absorption spectroscopy, MS = mass spectrometry, LIF = laser-induced fluorescence, CRDS = cavity ring-down spectroscopy.

the spectroscopic studies, the use of different IO absorption cross sections and instrumental resolution. However, recent studies[28,29,34,35] of the IO + IO reaction at ambient temperature are in good agreement, indicating a rate coefficient k_1 for the reaction

$$IO + IO \rightarrow \text{products} \qquad (1)$$

defined by $(-d[IO]/dt = 2k_1[IO]^2)$, in the range $k_1 = (8-10) \times 10^{-11}$ molecules^{-1} cm^3 s^{-1}. These recent results are somewhat higher than earlier measurements of k_1,[26,27,32,33] which were in the range $k_1 = (3 - 7) \times 10^{-11}$ molecules^{-1} cm^3 s^{-1}. Measurements of k_1 are summarized in Table 2. The temperature dependence of k_1 has been investigated by Sander[26] and by Harwood et al.,[29] both of whom used pulsed photolysis/UV−vis absorption techniques. Sander reports a negative temperature dependence to k_1 from 250 to 373 K, while Harwood et al. report a temperature independent k_1 over the same temperature range. This discrepancy is largely attributable to the different IO absorption cross sections used by these authors: the temperature dependencies of (k_1/σ_{IO}) determined by Sander and by Harwood et al. are in reasonably good agreement. Several authors have reported that k_1 is pressure-independent over the range 2−760 Torr at ambient temperature, in the absence of ozone.[26,28,29]

The products of the IO self-reaction are not well-known. The production of iodine atoms in reaction 1 is implied by a reduction in the rate coefficient k_1 observed in experiments carried out in an excess of ozone,[26,29] attributed to the rapid regeneration of IO radicals in reaction 3. Also, the formation of I_2 has been observed in studies of reaction 1.[28,29] No studies show that the I_2 and the I atom channels account for all of the IO self-reaction, however. Equally, no other channels of the IO + IO reaction have hitherto been identified. By analogy with the ClO and BrO self-reactions, four potential channels of the IO + IO reaction could exist:

$$IO + IO \rightarrow 2I + O_2 \qquad (1a)$$

$$\rightarrow I_2 + O_2 \qquad (1b)$$

$$\rightarrow OIO + I \qquad (1c)$$

$$IO + IO + M \rightarrow I_2O_2 + M \qquad (1d)$$

Comparison of the rate coefficients reported in the presence and absence of ozone indicates that iodine atom producing channels account for approximately 30% of reaction 1 at high (> 600 Torr) pressure and 298 K.[26,29] Since both channels 1a and 1c contribute I atoms, this implies that $\{(k_{1a} + {}^1/_2k_{1c})/k_1) \approx 0.3\}$. This value is in reasonable agreement with the branching ratio implied by studies of the iodine-photosensitized decomposition of ozone, which indicated that I atom channels accounted for 20 ± 7% of the IO self-reaction at 298 K and 760 Torr.[30] While the formation of I_2 has been observed in studies of reaction 1, the kinetics of I_2 formation were not consistent with the direct formation of I_2 in reaction channel 1b, and some I_2 formation is attributed to I atom recombination. Harwood et al.[29] placed an upper limit of 0.3 for the branching ratio k_{1b}/k_1, while both Sander[26] and Laszlo et al.[28] reported $k_{1b}/k_1 \leq 0.05$.

The visible absorption spectrum of OIO was recently reported by Himmelmann et al.,[36] following the flash photolysis of I_2/O_3 mixtures. The identification of OIO in this system indicates that reaction 1c may operate. Alternatively, the observed OIO may have originated from a reaction between IO and ozone:

$$IO + O_3 \rightarrow OIO + O_2 \qquad (7)$$

While OClO is known to form as a product of the ClO self-reaction,[37] OBrO is not formed from the self-reaction of ground state BrO radicals (although production of OBrO from the self-reaction of vibrationally excited BrO has recently been reported[38]) but can be formed by the slow reaction of BrO with O_3.[39,40] Formation of OIO from the IO self-reaction in the atmosphere would represent a null cycle with respect to ozone depletion *if* OIO subsequently underwent rapid solar photolysis to yield $O(^3P)$ + IO.

Reaction channel 1d, formation of the IO dimer, I_2O_2, is also possible by analogy with the other halogens. Formation of Cl_2O_2 from the ClO self-reaction is well-known,[37] and recent work in our laboratory has identified Br_2O_2 as a product of the BrO self-reaction.[41] The formation of I_2O_2 in the IO + IO reaction has been implied in previous studies from the low branching ratios for the production of I atoms and I_2 in this reaction. On this basis, Harwood et al.[29] indicate that formation of I_2O_2 could be the main product of the IO self-reaction. The absence of a pressure dependence to reaction 1 implies that the reaction channel 1d does not operate, or is not termolecular, or that channel 1d has reached its high-pressure limit at low pressures (a few Torr).

No definitive spectroscopic evidence for I_2O_2 has been reported. Sander[26] observed formation of an absorbing species at low (λ < 310 nm) wavelengths in the course of flash photolysis/UV absorption studies of the IO self-reaction. However, appearance of this absorption occurred on a considerably longer time scale than the decay of the IO radical, suggesting that this species may have been one of the higher iodine oxides, I_2O_5 or I_4O_9, formed by a multistep mechanism. Spietz et al.[42] have reported observing unattributed UV absorbers in the IO self-reaction system (in the presence of O_3) but have been unable to definitively identify the species responsible.

In this paper we present a determination of the absorption cross sections of the IO radical as a function of temperature, and an investigation of the temperature- and pressure depen-

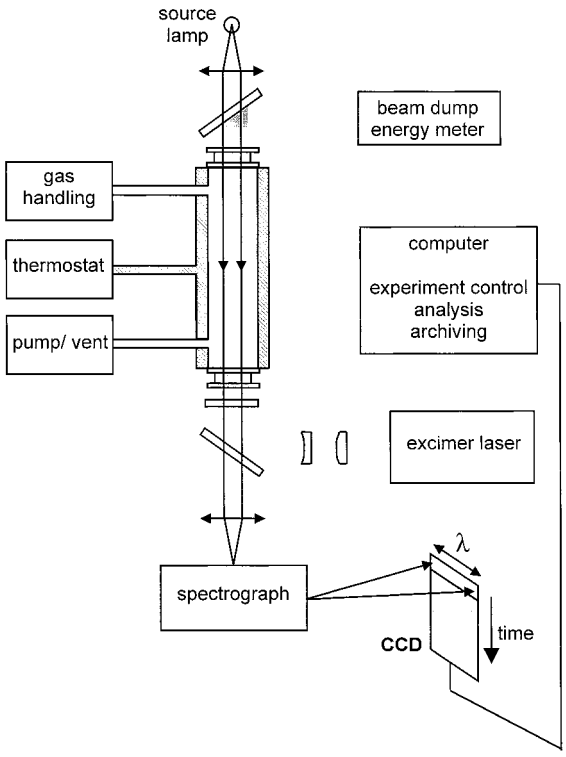

Figure 1. Schematic of the laser flash photolysis system. Source lamp light, having passed through the reaction cell, is dispersed and imaged across the top rows of the CCD array. Charge transfer is then used to move the signal generated by the incident light, representing a spectrum, into the storage region of the CCD, thereby enabling the rapid recording of sequential spectra of the reaction mixture.

dence of the kinetics of the IO self-reaction. The branching ratio for all four product channels of the IO self-reaction was also determined at 295 K and 760 Torr. In the accompanying paper,[43] we describe a study of the kinetics and products of the IO + BrO reaction. Results from the accompanying paper have been used to quantify branching ratios for the IO self-reaction. The atmospheric implications of the results obtained are briefly considered.

2. Experimental Details

Apparatus and Method. The IO absorption cross sections and the IO self-reaction were studied using laser flash photolysis coupled with time-resolved UV−vis absorption spectroscopy. Charge-coupled-device (CCD) detection was used to monitor the laser-initiated evolution and decay of chemical species. The apparatus has been described in detail previously;[40,41] therefore, only a brief description is given here. A schematic diagram of the apparatus is shown in Figure 1.

Precursor gas mixtures were prepared in a gas manifold using stainless steel mass flow controllers, and flowed continuously through a 1 m long jacketed quartz reaction cell. The reaction cell was temperature controlled using recirculating fluid from a thermostated bath, and cell temperatures in the range 200−350 K to within ±0.5 K could be maintained, as measured with a thermocouple placed in the gas flow. Gases were pumped through the reaction cell where necessary, allowing pressures from 50 to 760 Torr to within ±1 Torr to be maintained, as measured with a capacitance manometer.

Reactions were initiated using 193 nm pulsed excimer laser photolysis. The laser beam, initially with energies of 300−400 mJ/pulse and a pulse duration of 10−40 ns, was expanded and recollimated using cylindrical lenses, and passed, using dichroic mirrors longitudinally through the reaction cell filling the internal cell diameter (14.8 mm). The expansion recollimation and partial reflection of the laser beam reduced the laser fluence entering the reaction cell by a factor of 15−20, resulting in typical laser fluences in the cell of ca. 15−20 mJ cm^{-2}. The laser beam exiting the cell was terminated into a beam dump energy meter. The attenuation of the photolysis laser beam by absorbing species in the reaction cell was kept low and never exceeded 50%. At an attenuation of 50% of the laser beam, simulations showed that the resultant concentration gradients of photolytically generated species led to a slight deviation in apparent second-order rate coefficients of the order of 3%.

Concentrations of precursor gases, reactants, intermediate species, and products were monitored using UV−vis absorption spectroscopy. Analysis light from a 30W continuous output xenon arc lamp was collimated and passed along the long axis of the reaction cell, counterpropagating the laser beam. The analysis light beam was then focused onto the entrance slit of a 0.25 m focal length astigmatic Czerny−Turner spectrograph, fitted with three interchangeable diffraction gratings having 150, 300, and 600 grooves/mm. Wavelength-resolved analysis light from the spectrograph was imaged across the top of the CCD detector.

The CCD comprises an array of 1152 rows by 298 columns of light sensitive pixels, which convert incident light into photocharge. The device also has the facility to shift the photocharge rapidly and efficiently from row to row along the long axis of the array. The CCD was thus positioned with the short axis of the device in the dispersive focal plane of the spectrograph, perpendicular to the axis of fast charge transfer. The top 31 rows of pixels only were illuminated, and rows of photocharge, representing spectra of the transmitted analysis light intensity, were shifted down the device into an optically masked region. When the top row of charge had traversed the entire device, charge-transfer ceased and stored photocharge was read off and transferred to a PC for analysis. In this way, up to 1152 sequential transmission spectra of the reaction cell could be recorded. Charge-transfer rates of up to 1 MHz per row (1 μs per spectrum) were attainable. Wavelength coverage of up to 130 nm/spectrum was possible, depending upon the grating used. The spectrograph was regularly wavelength calibrated and the spectral resolution determined using the spectral emission lines from a low-pressure mercury lamp.

Absorption spectra of precursor gas mixtures were obtained by ratioing the analysis light intensity in the presence (I_t) and absence (I_o) of the gas mixture, according to Beer's law:

$$A_\lambda = \ln \{I_{o,\lambda} / I_{t,\lambda}\} \qquad \text{(i)}$$

For kinetic experiments, the photolysis laser was initiated during the charge-transfer process and time-resolved spectra were ratioed using an average prephotolysis intensity as I_o. Thus, spectra obtained show changes in the absorbance of the reaction mixture as a result of the photolysis laser pulse and subsequent chemistry.

Absorption spectra were analyzed by numerically fitting reference cross sections for the species of interest to all observed spectra. Thus, in kinetic experiments a spectrum was analyzed to determine species concentrations at each time point. Where the species of interest had structured absorption features, a "differential" spectral fitting technique was employed. This involved the high-pass filtering of both the observed spectrum and the reference cross sections, with fitting of the resulting structure using a linear least-squares method. This approach allowed the unequivocal identification and separate, accurate,

TABLE 3: Conditions of Precursor Species Employed and Resulting Peak IO Concentrations in This Work

species	concentration/molecules cm^{-3}
N_2O	$3.7-12.3 \times 10^{16}$
I_2	$1-3 \times 10^{14}$
CF_3I	$2-12.5 \times 10^{16}$
N_2	balance
peak IO (I_2 system)	$2-5 \times 10^{13}$
peak IO (CF_3I system)	$5-10 \times 10^{13}$

quantification of multiple structured absorbing species (such as IO) in the presence of other absorbers.

The experiments reported here were conducted using a 300 g/mm spectrograph grating, which gave a wavelength coverage of 65 nm. With 75 μm spectrograph entrance slits, this corresponded to a resolution (fwhm) of 1.13 nm. The CCD was operated at a spectral acquisition rate of 5×10^5 Hz, corresponding to a charge-transfer interval/spectral acquisition time of 2 μs.

Generation of IO Radicals. Two chemical systems were employed to generate IO radicals. In both cases N_2O was photolyzed at 193 nm to form $O(^1D) + N_2$. The excited oxygen atoms were then rapidly and exclusively collisionally quenched in an excess of nitrogen, and the resulting $O(^3P)$ atoms reacted with either CF_3I or I_2, forming IO radicals:

$$N_2O + h\nu \rightarrow N_2 + O(^1D) \quad (8)$$

$$O(^1D) + N_2 \rightarrow O(^3P) + N_2 \quad (9)$$

either

$$O(^3P) + I_2 \rightarrow IO + I \quad (10)$$

or

$$O(^3P) + CF_3I \rightarrow IO + CF_3 \quad (11)$$

N_2O (Distillers MG, 99%), N_2 (Distillers MG, 99.996%), O_2 (Distillers MG, 99.996%), and CF_3I (Fluorochem, 99%) were used as supplied. I_2 (Breckland Scientific, resublimed, >99%) was entrained in a flow of nitrogen passed through a trap containing glass wool interspersed with iodine crystals. Reactant concentration ranges are given in Table 3. The total flow of reagent gases through the reaction cell was chosen to ensure that a fresh gas mixture was photolyzed in each laser shot, while the flowout of reagents during a kinetic experiment was minimized. In both chemical systems (referred to hereafter as the I_2 or CF_3I systems), IO radicals were generated rapidly on the time scale of their subsequent loss, as evidenced by the prompt appearance of the characteristic structured absorption spectrum of the ($A^2\Pi \leftarrow X\ ^2\Pi$) vibronic transition between 400 and 470 nm. Subsequently, the IO absorption decayed on a time scale of hundreds of microseconds, as the IO radicals self-reacted. Typical peak IO concentrations ranged between $(2-10) \times 10^{13}$ molecules cm^{-3}. Typically, data from 100 laser shots were coadded, giving an IO detection limit (S:N = 1) of 1×10^{12} molecules cm^{-3}.

The use of two chemical systems for the generation of IO radicals allowed the investigation of different aspects of IO photochemistry. However, complications were associated with each IO generation system.

In the I_2 system, an excess of I atoms was generated relative to the IO radicals, both from reaction 10 and from the direct photolysis of I_2 at 193 nm:

$$I_2 + h\nu \rightarrow 2I \quad (12)$$

Moreover, because of the significant absorption cross section of iodine at 193 nm {σ (I_2, 193 nm) = 1.1×10^{-17} cm^2 $molecule^{-1}$},[44] the photolysis laser fluence and consequently the degree of N_2O photolysis were reduced. The need to preclude the creation of a significant concentration gradient of IO along the reaction cell (which would have distorted the observed kinetics) limited the molecular iodine concentration which could be employed. This resulted in a significant fraction (>10%) of the $O(^3P)$ atoms produced reacting with IO rather than I_2, and reducing the IO yield relative to photolytic O atom production:

$$O(^3P) + IO \rightarrow O_2 + I \quad (13)$$

$$(k_{13} = 1.2 \times 10^{-10}\ \text{molecules}^{-1}\,\text{cm}^3\,\text{s}^{-1})[28]$$

In contrast, in the CF_3I system, the much lower 193 nm absorption cross section of CF_3I ($\sigma(CF_3I, 193\ nm = 2.1 \times 10^{-21}$ $molecule^{-1}$ cm^2)[45] allowed higher CF_3I concentrations to be employed, such that $O(^3P)$ atoms reacted exclusively (>99.9%) with CF_3I. Thus, the yield of IO from this system, for an equivalent [N_2O] and laser fluence, was higher than for the I_2 system. However, some kinetic complications were observed: the production of IO in reaction 10 is accompanied by generation of CF_3 radicals, and the subsequent potential reactions of both CF_3 and CF_3I with IO are poorly characterized. Indeed, some evidence for a reaction between CF_3 and IO was obtained in this work, as discussed in the kinetics section, below.

3. Results

Determination of IO Absorption Cross Sections. The IO absorption cross sections, σ_{IO}, were determined using the CF_3I system. Thus, IO was generated and its spectrum recorded following photolysis of $N_2O/CF_3I/N_2$ mixtures, and in parallel experiments conducted under identical conditions, CF_3I was replaced by O_2. Substitution of O_2 for CF_3I led to formation of ozone in place of IO:

$$O(^3P) + O_2 + M \rightarrow O_3 + N_2 \quad (14)$$

The concentration of ozone was then determined using spectral fitting (in the Hartley band between 220 and 285 nm) with reference ozone cross sections.[3] The concentration of ozone produced was then equated to the concentration of $O(^3P)$ atoms produced from N_2O photolysis and subsequent $O(^1D)$ quenching, and hence to the flux through the $O(^3P) + CF_3I$ reaction in the IO experiment. This allowed quantification of the IO in the uncalibrated spectrum and hence the determination of absolute IO cross sections. Figure 2 shows the time-resolved *relative* IO concentrations, obtained by fitting an uncalibrated IO spectrum to successive spectra of the reaction mixture, along with absolute ozone concentrations obtained in the calibration experiment. The apparent noninstantaneous growth of the IO concentration is an experimental artifact arising from the time-averaging effect of the illumination of 31 rows in the temporal axis of the CCD array. This effect is readily accounted in determining the true maximum relative [IO] by including a temporal averaging function with a simple kinetics simulation.[46]

The nitrogen, oxygen and CF_3I concentrations employed (Table 3) were such that $O(^1D)$ atoms produced from N_2O photolysis were rapidly and exclusively quenched to $O(^3P)$ and that all $O(^3P)$ atoms reacted rapidly and stoichiometrically with oxygen or CF_3I. A small complication to the ozone experiments

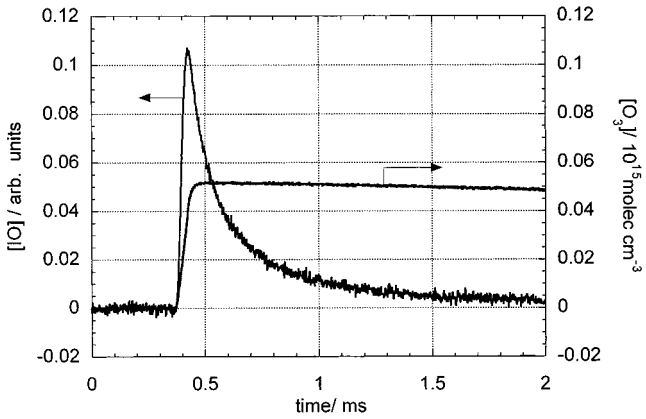

Figure 2. Temporal profiles for IO and O_3 recorded following photolysis of $N_2O/CF_3I/N_2$ and $N_2O/O_2/N_2$ mixtures, respectively. The rapid decay of IO radicals was followed by fitting the structure of the IO absorption spectrum.

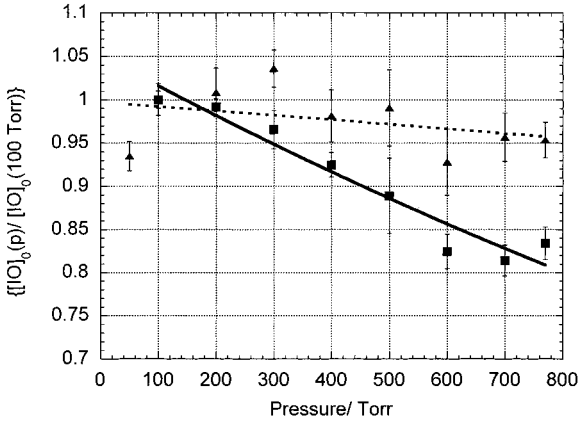

Figure 3. Initial IO yield for the CF_3I system measured as a function of pressure (relative to that at 100 Torr) at 295 K (filled triangles, dashed line) and at 220 K (filled squares, solid line).

was the additional source of O atoms produced from direct photolysis of molecular oxygen both inside and (mainly) outside of the reaction cell. Extracellular photolysis of atmospheric oxygen took place in the portion of the photolysis laser beam external to the cell but within the analysis beam path. This led to ozone production even in the absence of N_2O, which was determined in separate experiments and, with a small correction for laser fluence, subtracted from the ozone concentrations determined in the presence of N_2O. By minimizing the extracellular path length of the photolysis laser beam, the ozone correction was always small, and never exceeded 5% of the ozone concentrations produced from N_2O photolysis.

Having determined the $O(^3P)$ atom yield from N_2O photolysis and $O(^1D)$ quenching, the initial IO concentration from the $O(^3P) + CF_3I$ reaction could be determined. As shown by Gilles et al., the yield Φ of IO from the reaction of $O(^3P)$ with CF_3I is nonunity, and some other channel of this reaction must exist:

$$O(^3P) + CF_3I \rightarrow IO + CF_3 \quad (11a)$$

$$\rightarrow \text{other product} \quad (11b)$$

Hence, in determining $[IO]_0$:

$$[IO]_0 = [O(^3P)]_0\Phi = [O_3]_{obs}\Phi \quad (ii)$$

where

$$\Phi = k_{11a}/k_{11} \quad (iii)$$

The absorption cross sections of IO were calculated from the initial IO absorbance, the initial concentration of IO radicals $[IO]_0$, and the optical path length, l ($l = 98.2$ cm), according to the Beer−Lambert law. Thus,

$$\sigma_{(IO,\lambda)} = A_{(IO,\lambda,0)}/([IO]_0 l) \quad (iv)$$

Hence, from mechanism ii,

$$\sigma_{(IO,\lambda)} = A_{(IO,\lambda,0)}/([O_3]_{obs}\Phi l) \quad (v)$$

The nonunity yield of IO from the $O(^3P) + CF_3I$ reaction thus complicated the determination of $\sigma_{(IO)}$. However, the alternative chemical system for IO generation, $O(^3P) + I_2$ was not used since I_2 attenuates the photolysis laser beam, rendering $[O(^3P)]_0$ lower in the presence of iodine than would be the case in the presence of oxygen. In addition, the consumption of IO in reaction 13 ($O(^3P)$ + IO) leads to nonstoichiometric IO generation from $O(^3P)$ atoms, rendering calibration experiments of little value in this system.

The value of Φ for reaction 11 has been measured by Gilles et al.[47] who report $\Phi = 0.83 \pm 0.09$ at 100 Torr total pressure and by Vipond,[35] who reports $\Phi = 0.93 \pm 0.04$ at 2−4 Torr total pressure (both measurements at 298 K). Both results are supported by the recent suggestion of Yuan et al.[48] that the IO yield from reaction 11 may be pressure dependent if the reaction proceeds via a collisionally stabilizable CF_3IO^* intermediate:

$$O(^3P) + CF_3I \rightarrow CF_3IO^* \rightarrow IO + CF_3$$

$$\downarrow M$$

$$CF_3IO$$

Since the IO cross section determinations reported here were conducted at (760 ± 10) Torr, and the previous determinations of Φ were carried out at somewhat lower pressures, an investigation into the relative pressure dependence of Φ was carried out. As a measure of Φ, the relative initial IO yield was recorded as a function of pressure from 100 to 760 Torr, under otherwise identical conditions ($[N_2O]$, $[CF_3I]$ and laser fluence). This analysis assumes that the absorption cross section of IO σ_{IO} is itself pressure independent. At 295 K, no significant variation in the IO yield, and hence Φ was observed with pressure. However, at lower temperatures (220 K), a reduction in the initial IO yield of approximately 20% was observed as the pressure was increased from 100 to 760 Torr. Figure 3 shows the relative initial yields of IO from these experiments, normalized to the IO yield at 100 Torr. At intermediate temperatures, the pressure dependence of Φ was found to vary approximately linearly. Thus, using the temperature-independent, 100 Torr value of $\Phi = 0.845$ recommended by Gilles et al.,[47] the 760 Torr value of Φ was parametrized using:

$$\Phi\ (760\ \text{Torr}) = 0.845(1 + (T - 295)/450) \quad (vi)$$

The value of Φ from this parametrization was used, along with the ozone calibration results and the optical path length, to convert the IO absorption spectrum into absorption cross sections using equation v. The relative IO decay trace obtained from differential fitting of the uncalibrated IO spectrum was used to determine the fraction of the peak concentration of IO present in the uncalibrated spectrum, thereby accounting for IO loss during the spectral recording.

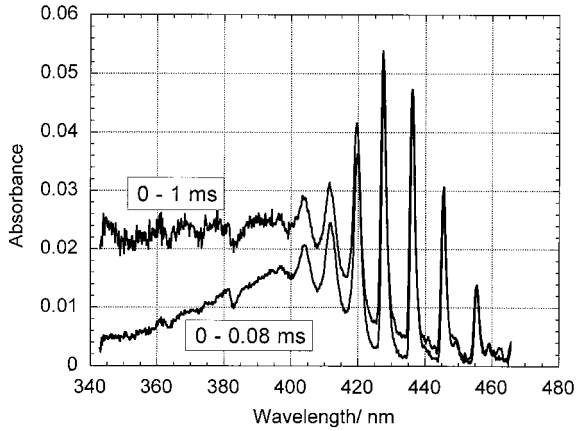

Figure 4. Postphotolysis relative to pre-photolysis absorption spectra of a $N_2O/I_2/N_2$ reaction mixture recorded over 80 μs and 1 ms postphotolysis time periods.

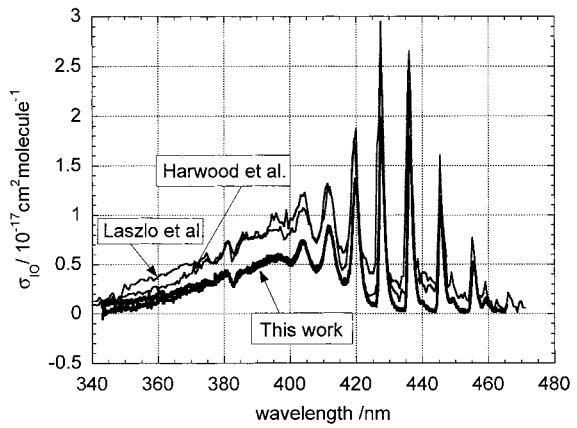

Figure 5. Upper and lower limits for the absorption cross sections of IO determined in this work at 295 K. Also shown are the IO spectra reported by Laszlo et al.[28] and by Harwood et al.[29]

The form of the observed IO absorption spectrum was found to vary with time following photolysis. This is shown in Figure 4, in which a spectrum recorded over the first 80 μs following photolysis is compared to a spectrum recorded over the first 1 ms following photolysis. In Figure, the 1 ms spectrum, with lower [IO], has been normalized using the IO differential structure to contain the same contribution from IO as the 80 μs spectrum. The observed spectral evolution was attributed to the formation of an additional absorbing or scattering species with an apparently monotonically increasing absorption to decreasing wavelengths. This species, hereafter referred to as P, was formed on the time scale of the IO decay.

The apparent spectrum of P was deconvolved from that of IO by performing a scaled subtraction of a spectrum recorded immediately following photolysis (0−500 μs), containing mostly IO, from one recorded at a later time after photolysis (500−1000 μs), containing mostly P. The differential structure of IO was used to scale the early (0−500 μs) spectrum to the late (500−1000 μs) spectrum, and the former was then subtracted from the latter, thereby giving a spectrum of species P with no contribution from IO. It was not possible to reverse this procedure to obtain a pure spectrum of IO since no independent measure of relative [P] (as was provided by the IO structure) was available. Two approaches were therefore adopted to acquire upper and lower limits for the IO absorption spectrum (and hence cross sections) in the absence of other absorbers. An upper limit to the IO spectrum was acquired by recording spectra for a very short period of time immediately following photolysis, when IO concentrations were at their maximum and those of P minimized. A time period of 0−20 μs after photolysis was found to be the shortest commensurate with an acceptable S:N ratio. This spectrum represented an upper limit since the presence of any other absorbers would indicate that the true IO spectrum was infact lower. A lower limit for the IO spectrum was obtained by assuming that below some critical wavelength λ_c, the observed absorption arose solely from species P. As a spectrum of P had been recorded, the appropriate contribution from this species to the IO absorption could be removed by fitting the spectrum of P to the measured absorption at wavelengths below λ_c. In practice, λ_c was set to 340 nm by inspection of observed spectra. This procedure gave a spectrum representing a lower limit since any contribution to the total absorption arising from IO at wavelengths shorter than λ_c would have resulted in oversubtraction of P. The upper and lower limits obtained for the IO spectra are shown as cross sections in Figure 5. The two limits covered a very narrow range, and the mean

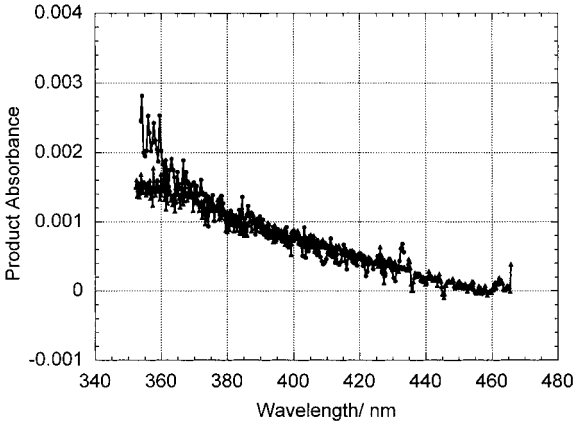

Figure 6. Absorption spectra of species "P" as recorded in the CF_3I and I_2 systems. The spectra have been arbitrarily scaled to be of similar magnitude.

was taken to determine final IO absorption cross sections. The differential IO cross sections, used to convert the absorption spectra to cross sections in the subsequent kinetics experiments, were unaffected by the presence or subtraction of species P.

A similar apparent absorbing species to P was also observed in the I_2 system, in addition to IO. An identical spectral separation procedure was performed, although quantification of σ_{IO} in this system was not possible since $[IO]_0$ could not be independently determined, as discussed above. The spectra of P recorded in each system are shown in Figure 6. The spectra have been arbitrarily scaled to be of similar magnitude. The identity of species P is discussed in the context of the reaction products, below.

The final IO cross sections determined at ambient temperature (295 ± 3 K) and at 1.13 nm fwhm instrumental resolution are plotted in Figure 5. The first series of vibrational bands of the IO ($A^2\Pi \leftarrow X^2\Pi$) transition from (7,0) to (0,0) are well-defined, and the (3,1), (2,1), and (1,1) hot bands can be resolved at 448.9, 459.0, and 469.7 nm, respectively. The IO cross section at 427.2 nm, the peak of the (4,0) band, is $(1.9 \pm 0.17) \times 10^{-17}$ $molecules^{-1}$ cm^2, and the cross section at 396.5 nm, the peak of the (resolution-independent) IO shoulder is $(5.7 \pm 0.5) \times 10^{-18}$ $molecules^{-1}$ cm^2. Band assignments were taken from ref 29. The errors quoted are a combination of the statistical (2σ) variation in the IO cross section determinations and the uncertainty in the value of Φ,[47] which is the major source of potential systematic error. The IO cross sections are listed as a function of wavelength in Table 4S (Supporting Information).

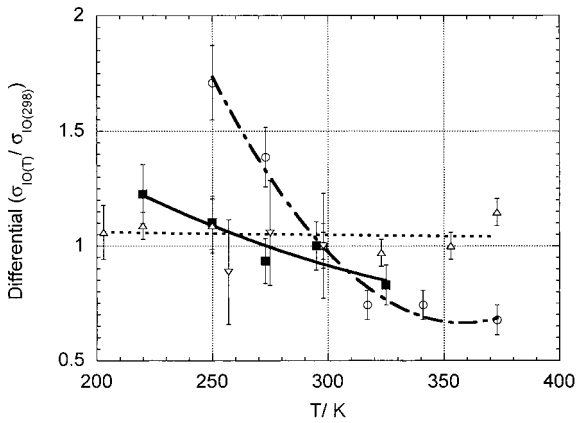

Figure 7. Temperature dependence of differential IO cross sections from this work, recorded over the wavelength range 400−470 nm (filled squares, solid line), compared with the results of Sander[26] (open circles, dot−dash line) and Harwood et al.[29] (CF_3I system, open triangles, dashed line; I_2/O_3 system, inverted open triangles) Plotted relative to 295−298 K value.

TABLE 5: Reactions Included in the Kinetic Model Used to Determine k_1

reaction	k (295 K)/ molecules^{-1} cm^3 s^{-1}	ref
$O(1D) + N_2 \rightarrow O(^3P) + N_2$ (14)	2.6×10^{-11}	De More et al.[3]
$O(^3P) + I_2 \rightarrow IO + I$ (15)	1.4×10^{-10}	De More et al.[3]
$O(^3P) + IO \rightarrow I + O_2$ (18)	1.2×10^{-10}	Laszlo et al.[28]
IO + IO → products (1)	optimized	

The IO cross sections were measured as a function of temperature at 220, 250, 273, 295, and 325 K. The differential IO cross section, as used to quantify IO in the kinetic experiments, was found to increase with decreasing temperature, by approximately 40% between 325 and 220 K. The relative differential IO cross section as a function of temperature is shown in Figure 7, together with the results from other studies. The temperature dependence of the differential cross section reported here is in contrast to the temperature-independent σ_{IO} reported by Harwood et al.[29] and less pronounced than the negative temperature dependence reported by Sander.[26]

Kinetics of the IO Self-Reaction. The rate coefficient for the IO self-reaction was determined from the rate of loss of IO radicals, generated from the $O(^3P) + I_2$ reaction 10. IO decay traces were generated by fitting the IO reference cross sections to successive IO absorption spectra, recorded on each row of the CCD at 2 μs time intervals, using the differential fitting technique. The decay traces so obtained were thus unaffected by the formation of species P or any other products. The decay of IO radicals in the I_2 system was found to follow second-order kinetics, with slight deviations due to the $O(^3P)$ + IO (reaction 13) and the flowout of IO radicals from the reaction cell. To account for these, and for the distortion to the decay traces imparted by the CCD time-averaging effect, a simple model of the reaction system was constructed using the FACSIMILE[49] numerical integration package, incorporating the reactions listed in Table 5 and a simulation of the temporal averaging kernel. Within the model, the concentration of photolytically produced $O(^1D)$ atoms and the value of k_1 were optimized to minimize the sum of squares of residuals between calculated and observed decay traces. A typical decay trace and optimized fit are shown in Figure 8.

The overall rate coefficient k_1 for the IO self-reaction was found to be $(8.2 \pm 1.0) \times 10^{-11}$ molecules^{-1} cm^3 s^{-1} at 295 ± 3 K and 760 ± 10 Torr. The value is the mean of 37 determinations, each of which results from between 50 and 100 laser shots, and the error represents $\pm 2\sigma$ statistical only. Incorporation of the 11% uncertainty in the differential IO cross sections gives $k_1 = (8.2 \pm 1.3) \times 10^{-11}$ molecules^{-1} cm^3 s^{-1}. The self-reaction rate coefficient was measured as a function of pressure between 100 at 760 Torr at 295 and 220 K. No pressure dependence to k_1 was observed at either temperature. The temperature dependence of the IO + IO reaction rate coefficient was investigated with determinations of k_1 at 222, 235, 250, 273, 295, and 325 K. The temperature-dependent IO absorption cross sections reported above were used to quantify [IO], with interpolation performed to determine σ_{IO} at temperatures intermediate to those at which the cross sections were measured. The temperature-dependent values of k_1 obtained are given in Table 6, and plotted in Arrhenius form in Figure 9. The reaction exhibits a weak negative temperature dependence, which is described by

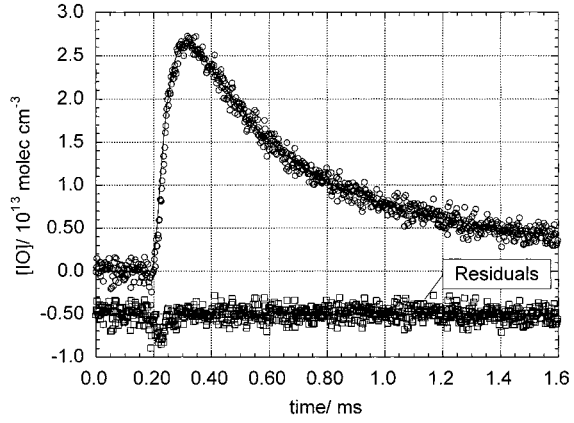

Figure 8. Typical IO decay trace (I_2 system), optimized fit and residuals (offset).

TABLE 6: Rate Coefficients Obtained for the IO Self-Reaction as a Function of Temperature

	rate coeff × 10^{11}/molecules^{-1} cm^3 s^{-1}	
temperature/K	k_1	$\pm 2\sigma$
325	7.51	0.80
296	8.18	1.0
273	9.44	0.42
250	11.6	1.8
235	8.14	1.6
222	10.4	2.2

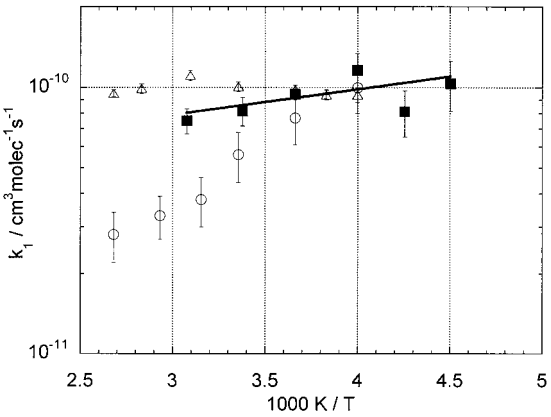

Figure 9. Arrhenius-fit to the temperature-dependent IO self-reaction rate coefficients determined in this work (filled squares). Temperature-dependent values of k_1 reported by Sander[26] (open circles) and by Harwood et al.[29] (open triangles) are also shown.

$$k_1 = (4.1 \pm 3.4) \times 10^{-11} \exp\{(220 \pm 230)/T\}$$
$$\text{molecules}^{-1}\,\text{cm}^3\,\text{s}^{-1} \quad \text{(vii)}$$

Errors on both Arrhenius parameters are $\pm 2\sigma$.

Kinetics of the IO decay recorded using the O + CF_3I reaction 11 as the source of IO deviated significantly from second-order and showed enhanced IO removal rates. The decay of IO in this system could be simulated by incorporation of an additional first-order loss of IO into the reaction scheme given in Table 5. The kinetics were equally well-described by adding either reaction 15 or 16 to the reaction scheme:

$$\text{IO} + \text{SRP} \rightarrow \text{products} \quad (15)$$

$$\text{IO} + \text{CF}_3 \rightarrow \text{products} \quad (16)$$

Where SRP = a product of the IO self-reaction. The kinetics of IO in the CF_3I system were not considered further due to the many poorly characterized reactions which could occur.

Products of the IO Self-Reaction. The four potential product channels of the IO self-reaction (by analogy with other halogen monoxide self-reactions) are discussed in turn below:

(a) IO + IO → I + I + O_2. Since I atoms absorb in the vacuum UV, it was not possible to detect I atoms directly using this apparatus. However, it was in theory possible to quantify the production of I atoms in reaction 1 by addition of excess ozone. The rapid regeneration of IO radicals from I atoms via reaction 3 in the presence of excess ozone would reduce the observed IO self-reaction rate coefficient (measured as loss of IO radicals) due to the effective suppression of I atom producing channels. Thus, measurement of k_1 with and without excess ozone would have determined a branching ratio for I atom producing channels. Alternatively, the catalytic loss of ozone would itself have been an indicator of the I atom yield during the IO self-reaction. In practice, trial experiments in which sufficient ozone was added to the precursor gas mixtures to rapidly reconvert I atoms into IO resulted in yellow-white solid deposits on the walls and windows of the apparatus, severely degrading the optical performance of the system and precluding the conduct of useful experiments. This behavior is consistent with that reported by other groups: Harwood et al.[29] reported the formation of aerosol and deposition of a brown solid in a mixture of I_2 and O_3; similar effects have been reported in several other studies.[26,30,35] This behavior is attributed to the formation of higher iodine oxides, I_2O_5 and I_4O_9, in a thermal (i.e. nonphotoinitiated) reaction of I_2 with O_3.[30] As a result of these complications, the branching ratio for channel 1a could not be directly quantified: an indirect determination is described below.

(b) IO + IO → I_2 + O_2. The formation of molecular iodine was observed in the IO self-reaction system, and studied using the O(^{3}P) + CF_3I reaction as the source of IO. This system was chosen since excess I atoms were present in the O + I_2 system, providing a significant additional source of I_2 from termolecular I atom recombination. I_2 concentration vs time profiles were obtained by differential fitting of reference I_2 cross sections to the structured I_2 absorption over the wavelength region 520−580 nm. Differential reference I_2 cross sections were generated from absorption spectra of I_2/N_2 mixtures recorded at the same resolution as kinetic experiments, and reference I_2 cross sections were calibrated using lower resolution (spectrally smooth) I_2 cross sections taken from the literature.[50] Typical IO and I_2 profiles obtained in this way are shown in Figure 10.

Notwithstanding the use of O(^{3}P) + CF_3I as the source of IO radicals in these experiments (i.e., a chemical system which does not produce an excess of I atoms) several potential sources could account for the observed I_2. Modeled I_2 profiles for each of the following potential I_2 formation mechanisms are shown in Figure 10:

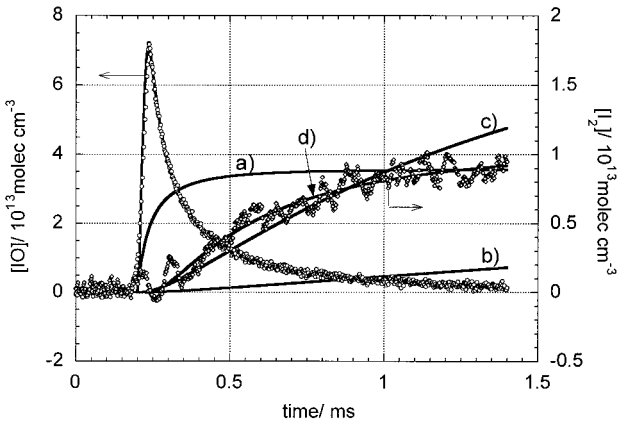

Figure 10. IO and I_2 concentration profiles, CF_3I system. The I_2 data has been smoothed via application of a running average for clarity. Also shown are simulated I_2 profiles predicted for four possible I_2 formation mechanisms (a−d) referred to in the text.

(a) direct production of I_2 from reaction 1b,

$$\text{IO} + \text{IO} \rightarrow \text{I}_2 + \text{O}_2 \quad (1b)$$

(b) I atom formation in reaction 1a, followed by recombination,

$$\text{IO} + \text{IO} \rightarrow 2\text{I} + \text{O}_2 \quad (1a)$$

$$\text{I} + \text{I} + \text{M} \rightarrow \text{I}_2 + \text{M} \quad (17)$$

(c) I atom formation in reaction 1a followed by a reaction between I atoms and some other product of the IO self-reaction (denoted SRP), as suggested by Laszlo et al.,[28]

$$\text{IO} + \text{IO} \rightarrow 2\text{I} + \text{O}_2 \quad (1a)$$

$$\text{IO} + \text{IO} \rightarrow \text{SRP} \quad \text{(e.g., (1d))}$$

$$\text{I} + \text{SRP} \rightarrow \text{I}_2 + \text{products} \quad (18)$$

(d) I atom formation in reaction 1a, followed by IO-catalyzed iodine atom recombination, by analogy with the behavior of Br atoms, and as suggested by Harwood et al.,[29]

$$\text{I} + \text{IO} + \text{M} \rightarrow \text{I}_2\text{O} + \text{M} \quad (19)$$

$$\text{I} + \text{I}_2\text{O} \rightarrow \text{I}_2 + \text{IO} \quad (20)$$

As shown in Figure 10, the observed formation kinetics of I_2 were inconsistent with the direct mechanism a producing I_2 from reaction 1b. The observed rate of I_2 formation was not proportional to $[IO]^2$, as would be expected from the direct channel 1b. Moreover, the absolute amount of I_2 formed amounts to a small fraction of the IO undergoing self-reaction: the I_2 profile for mechanism (a) was generated using a branching ratio (k_{1b}/k_1) of 0.22. In contrast, the alternative mechanism b, producing I_2 from the recombination of I atoms produced in reaction 1a, led to I_2 formation on a much slower time scale than that observed, even assuming that reaction 1 produced exclusively 2I + O_2. Thus, this mechanism alone could not account for the observed I_2. Mechanism c, producing I_2 from the secondary reaction of I atoms with some other product of reaction 1 could produce a modeled I_2 profile more closely resembling the observed I_2. In simulation c, the branching ratios for reaction 1 were set at those reported by Harwood et al.;[29]

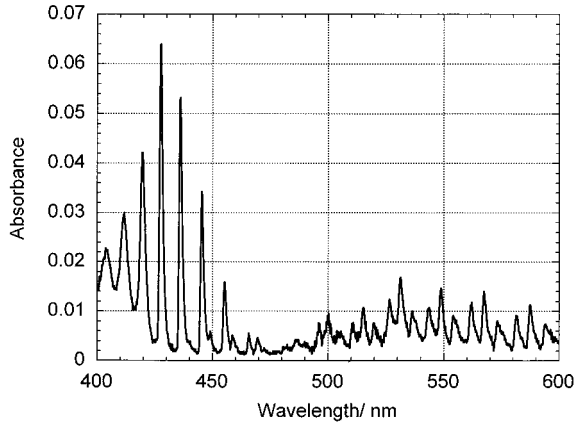

Figure 11. Post-photolysis absorption spectrum showing the distinctive bands of IO (between 400 and 470 nm) and OIO (between 495 and 600 nm). From the CF_3I system.

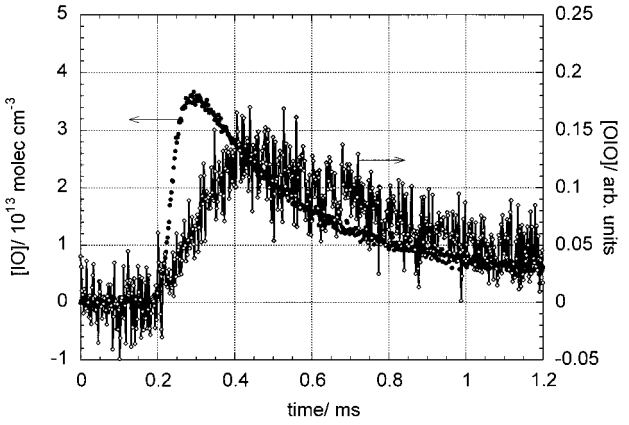

Figure 12. Typical temporal profiles for IO and OIO, determined using differential spectroscopy. From the I_2 system.

the product SRP was assumed to be IOOI, and the rate of reaction 18 was allowed to vary to optimize the fit to the I_2 profile. Finally, mechanism d, producing I_2 from IO catalyzed I atom recombination, gave the best fit of modeled to observed I_2 formation profiles. The rate coefficients for reactions 19 and 20 were both allowed to vary to optimize the fit, and returned values of $k_{19} = 1.7 \times 10^{-10}$ and $k_{20} = 2.1 \times 10^{-10}$ molecules^{-1} cm^3 s^{-1}, at 295 K and 760 Torr. The possibility of a combination of mechanisms operating cannot be ruled out, in which case the rate coefficients k_{19} and k_{20} represent upper limits.

These results indicate that direct production of I_2 in reaction 1b is minor, and are consistent with the upper limit of $k_{1b}/k_1 \leq 0.05$, as reported by Sander[26] and by Laszlo et al..[28] In addition, some enhancement to the rate of I_2 formation over simple I atom recombination must operate, and mechanism d is the most likely candidate.

(*c) IO + IO → OIO + I.* Examination of post-photolysis spectra obtained for both chemical systems used to generate IO showed that, in addition to the absorption spectra of IO and I_2, a progression of bands extending from 495 nm to above 600 nm was present. These features, shown along with the IO bands in Figure 11, were identical in wavelength and appearance to those originally reported by Himmelman et al.,[36] and were attributed to OIO. Differential fitting was used, with an uncalibrated OIO spectrum, to obtain the temporal profile of relative [OIO], shown along with an IO trace in Figure 12. OIO was observed to grow in and decay in these experiments on a similar time scale to IO, but with clearly independent kinetic behavior.

By analogy with OClO and OBrO, potential sources of OIO include reactions 1c and the reaction 7 of IO with ozone. However, no ozone was present in any of these experiments, showing that reaction 7 is not the source of observed OIO in this work. In previous studies, Himmelmann et al.[36] observed OIO in a I_2/O_3 photolysis system and attributed OIO to a product of either the IO + O_3 or the IO + IO reaction. Subsequently, we reported[51,52] that OIO was a product of the IO self-reaction via observation of OIO in the absence of ozone, details of which are given below. Ingham et al.[31] have also observed OIO production following the formation of IO in the O + I_2 reaction. Ingham et al. employed ozone as the photolytic source of O atoms for IO production, but showed that ozone was completely removed in the photolysis process and thus absent during the IO decay.

These observations all imply that OIO is indeed a product of reaction 1. However, alternative reactions which could act as OIO sources include the (probably termolecular) combination of O(^{3}P) and IO. In this work, the majority of OIO formation (>90%) was observed to take place beyond the calculated lifetime of O(^{3}P) atoms implying that O(^{3}P) + IO is not the OIO source.

The reaction of I atoms with an IO dimer of the form IOIO could also provide a source of both OIO and I_2 (analogous to mechanism iii above.) However, the rate of formation of OIO via this mechanism, which would be equal to the rate of I_2 formation, shown in Figure 10, was much too slow to account for the observed rate of OIO production. We therefore conclude that OIO is a product of the IO self-reaction.

Absolute absorption cross sections for OIO were unknown prior to this work, preventing direct quantification of the branching ratio for OIO production in reaction 1. However, a lower limit for the OIO absorption cross sections was derived assuming a unity branching ratio for OIO formation in reaction 1, and that no OIO loss occurred. At the peak of the (5,1,0) band[36] at 549 nm this gave $\sigma(\text{OIO}) \geq 4.15 \times 10^{-18}$ molecules^{-1} cm^2.

The formation of OIO was also observed from the IO + BrO reaction, as described in the accompanying paper:[43]

$$\text{IO} + \text{BrO} \rightarrow \text{Br} + \text{OIO} \qquad (21)$$

The branching ratio for OIO formation from reaction 21 was used to constrain the branching ratio for production of OIO in reaction 1 and hence the OIO absorption cross sections. This analysis, details of which are given in the accompanying paper,[43] indicated that the branching ratio to for OIO production from the IO self-reaction lies within the range:

$$0.30 \pm 0.05 \leq k_{1c}/k_1 \leq 0.46 \pm 0.08$$

corresponding to a range of OIO cross sections (at the peak of the (5,1,0) band at 549 nm, with 1.13 nm fwhm resolution) of

$$1.29 \pm 0.22 \geq (\sigma(\text{OIO}) \times 10^{17}) \geq 0.87 \pm 0.15$$

The range in values of k_{1c}/k_1 and σ(OIO) correspond to the range of possible branching ratios for the production of OIO + Br from reaction 21, and the errors in each value reflect the propagated statistical uncertainty (2σ) in the relative [OIO], [BrO], and [IO] used in these calculations. The wavelength-dependent OIO absorption cross sections corresponding to the center of the calculated ranges of peak cross section are listed in Table 7S (Supporting Information). The range in peak OIO cross section reported here is lower than the lower limit of

2.7×10^{-17} cm^2 recently reported for σ_{OIO} at 548.6 nm by Ingham et al.;[31] this point is discussed more fully below.

OIO was a transient species in all experiments, removed over a period of hundreds of microseconds. Since flowout and heterogeneous loss of OIO on the walls of the reaction vessel were negligible on this time scale, OIO must undergo further reaction. Proportionately higher peak OIO concentrations, for a given initial [IO], were observed using O(^{3}P) + CF_3I as the source of IO relative to using O + I_2 as the source of IO. This may indicate that reaction of OIO with I atoms, present in excess in the I_2 system, was at least in part responsible for the removal of OIO. If this reaction occurs and leads to rapid regeneration of IO (reaction 23a), rate coefficients for the IO self-reaction determined from the rate of loss of IO radicals will be underestimates.

$$\mathrm{I + OIO \rightarrow IO + IO} \quad (23a)$$

$$\rightarrow \text{products (not IO)} \quad (23b)$$

Several further possibilities exist for the secondary loss of OIO in both reaction systems including:

$$\mathrm{IO + OIO + M \rightarrow I_2O_3 + M} \quad (23)$$

$$\mathrm{OIO + OIO \rightarrow} \text{ products} \quad (24)$$

$$\mathrm{CF_3 + OIO \rightarrow} \text{ products} \quad (25)$$

$$\mathrm{CF_3I + OIO \rightarrow} \text{ products} \quad (26)$$

$$\mathrm{I_2 + OIO \rightarrow} \text{ products} \quad (27)$$

Several permutations of some or all of reactions 22−27 could be used to model the observed temporal behavior of OIO in both chemical systems for the production of IO, but the exact fate of OIO in these experiments could not be unequivocally elucidated. Moreover, the high concentrations of reactive radical species present in this system give rise to an environment atypical of the atmosphere, in which the apparent reactivity of OIO may not be reproduced.

(d) IO + IO (+ M) → I_2O_2 (+ M). The experiments described above show that I_2 is not a significant product of the IO self-reaction, and that channel 1c (formation of OIO + I) can account for up to (46 ± 8%) of reaction 1). In addition, previous studies[26,29,30] of reaction 1 indicate that production of I atoms is not the dominant channel of reaction 1 at high pressure ($k_{1a}/k_1 \leq \approx 0.3$ at 760 Torr/295 K). Thus, a significant fraction of the flux through the IO self-reaction is unaccounted for, possibly implying that channel 1d occurs. An unattributed spectrally smooth apparent absorption feature produced in the IO self-reaction system was also observed in the course of these experiments, as discussed above. This feature could result from molecular absorption or from light scattering through aerosol formation, and, for the reasons given below, we have tentatively identified the absorbing/scattering species (referred to as "P" above) as I_2O_2.

The concentration profile obtained for P in the I_2 system is compared with that predicted for an inert product of the IO self-reaction in Figure 13. The formation kinetics of species P are consistent with those predicted for channel 1d, supporting the assignation of P as I_2O_2. Previous studies of IO kinetics[26] have observed aerosol formation: however, this observation took place on a much longer time scale than that of the IO decay. Species P in this system is formed on a time scale similar to that of the IO decay. At long times (>1.6 ms in this system)

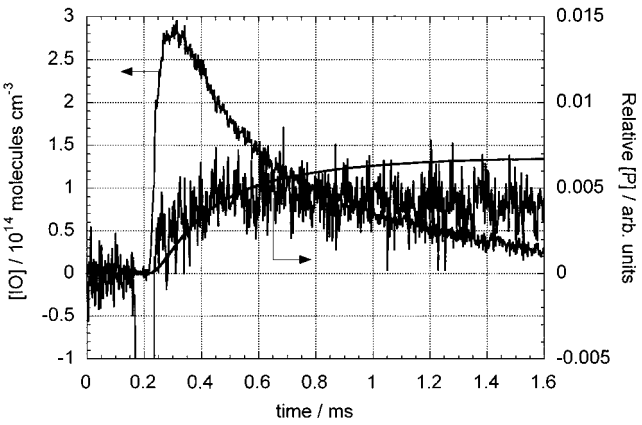

Figure 13. Temporal profile for IO and species "P" in the I_2 system. Also shown is the temporal profile predicted for an inert product of the IO self-reaction, arbitrarily scaled.

some loss of species P was apparent, which would not be expected if P were aerosol. The final absorption of P was lower (relative to $[IO]_{t=0}$) in the I_2 system than in the CF_3I system, suggesting that reaction between I atoms, present in excess in the I_2 system, and P may occur. If species P was IOOI, this reaction would produce I_2 and IOO, which, by analogy to ClOO[37] and BrOO,[41] could decompose giving I + O_2:

$$\mathrm{I + IOOI \rightarrow I_2 + IOO} \quad (31)$$

Several alternative chemical candidates for the identity of species P were considered. Products of reactions of CF_3 or CF_3I were discounted, as the same absorption was observed in both the I_2 and the CF_3I systems. I_2O was also discounted on the basis of the recently reported I_2O spectrum.[53] Another possibility was I_2O_3, formed from the reaction of IO with OIO:

$$\mathrm{IO + OIO + M \rightarrow I_2O_3 + M} \quad (23)$$

However, occurrence of this reaction is inconsistent with the observed second-order decay kinetics for IO. We therefore conclude that the most likely identity for species P is I_2O_2. The isomeric nature of I_2O_2 (IOIO vs. IOOI) is considered further in the discussion of the branching ratio of the IO self-reaction.

4. Discussion

IO Absorption Cross Sections. The ambient temperature IO absorption cross sections obtained in this work are compared with those reported by Laszlo et al.[28] and Harwood et al.[29] in Figure 5, and with other literature values for the cross section at the peak of the (4,0) band at 427.2 nm in Table 1. The general form of the calibrated absorption spectrum of IO is similar to that reported in the earlier studies;[26,29] however, two significant differences are apparent. First, the difference in the size of the structural features shown in Figure 5 arises largely from the different spectral resolutions employed: Harwood et al. and Laszlo et al. worked at 0.44 and 0.3 nm fwhm, respectively, while this work was conducted at 1.13 nm fwhm. When the cross sections reported by Harwood et al. were smoothed to the resolution of this work, the magnitudes of the resulting differential cross sections agree to within 2%. Second, the cross sections obtained in this work are smaller in absolute magnitude than those from the previous studies, particularly at shorter wavelengths, by up to 50%. This difference is attributed to the absorption of species P (I_2O_2) which underlies the short wavelength IO continuum absorption and which was separated from the IO absorption in this work.

Considering also the single wavelength IO cross sections reported for the 427.2 nm peak, another potential source of discrepancy arises from the $O(^3P) + IO$ reaction 13. The occurrence of this reaction, which has recently been shown to be extremely rapid ($k_{13} = 1.2 \times 10^{-10}$ molecule^{-1} cm^3 s^{-1}),[28] was not taken into account in some of the early determinations of σ_{IO}.[26,27] If reaction 13 did occur to a significant extent in early determinations of σ_{IO}, it would have the effect of reducing the IO concentration and hence lead to underestimation of the IO cross sections for a given calibrated O atom signal. The $O(^3P) + IO$ reaction was characterized and taken into account by Laszlo et al.[28] who used a N_2O/I_2 system to generate IO radicals and to calibrate σ_{IO}. The calibration of initial O atom concentration in the work of Laszlo et al. was afforded by the substitution of O_2 for I_2 and the generation of O_3 as a measure of $[O(^3P)]_0$. However, Laszlo et al. do not mention any correction to the IO yield which would result from the reduction in 193 nm laser fluence in the presence of I_2. In the absence of such a correction, the IO cross sections would be slightly underestimated and we note that the value for peak σ_{IO} reported by Laszlo et al. is lower than that from other studies at the same spectral resolution and that of Harwood et al.[29] at lower resolution.

The temperature dependence of the IO cross sections measured in this work is compared with the previous measurements of Sander[26] and Harwood et al.[29] in Figure 7. The IO absorption cross sections have been found to exhibit a negative temperature dependence in this work. Harwood et al., who also used the $O + CF_3I$ reaction to generate IO, adopted the temperature-independent value of Φ measured at 100 Torr by Gilles et al.[47] and applied this value at ambient pressure, and found the IO cross sections to be temperature independent. We have found that Φ displays a pressure dependence between 100 and 760 Torr at low temperatures, and that the 100 Torr value[47] must therefore be corrected according to equation vi before it can be applied at ambient pressure. The disparity in the temperature dependence of σ(IO) between the results of Harwood et al.[29] and this work can be accounted for by the different Φ values employed. In addition to the N_2O/CF_3I experiments, Harwood et al. conducted a limited number of measurements of the temperature dependence of the IO cross section using an I_2/O_3 system to generate IO radicals; however, the results from these experiments (also shown in Figure 7) are too scattered to confirm a definite trend. Sander observed a pronounced negative temperature dependence to the cross section at temperatures below 317 K. While reasons for the disagreement with this work are uncertain, it is possible that a temperature dependence to the rate coefficient of reaction 13, $O(^3P) + IO$, may explain the discrepancy.

Kinetics of the IO Self-Reaction. Previous measurements of the rate coefficient of the IO self-reaction are compared with the results of this work in Table 2 and in Figure 9. The ambient temperature value of k_1 obtained in this work is in good agreement with the most recent determinations.[28,29,34] The values of k_1 obtained in the earlier studies[26,27,32] are somewhat lower than that reported here. Reasons for the discrepancy are unclear: the IO cross sections used by Sander[26] are slightly smaller than the resolution used (0.17 nm fwhm) would suggest in comparison with other measurements[28,29] (Table 1), but not sufficiently so to account for the difference in rate coefficient. Barnes et al.[32] employed mass-spectrometric detection of IO to measure k_1, thus avoiding any dependence of their kinetics results upon σ(IO). The rate coefficient determined by Vipond[35] ($(9.3 \pm 1.0) \times 10^{-11}$ molecules^{-1} cm^3 s^{-1}) via I atom resonance fluorescence at very low (2−4 Torr) pressures is in agreement with the value reported here. Moreover, the value of k_1 reported by Vipond indicates that the pressure-independence determined for the IO self-reaction rate coefficient in the absence of ozone extends beyond the pressure range studied in the flash photolysis/UV absorption experiments (50 Torr and above) to the low pressures used by Barnes et al. (a few Torr).

The only two previous measurements of the temperature dependence of the IO self-reaction rate coefficient[26,29] were both performed using the flash photolysis/UV absorption technique, analogous to this work. Thus, the temperature dependence obtained for k_1 in these studies is directly dependent upon the temperature dependence of the IO cross sections employed. Harwood et al.[29] found both k_1 and σ(IO) to be temperature independent, while Sander[26] found both to exhibit a negative temperature dependence. Comparison of the k/σ values confirms that the trends obtained for k_1 with respect to temperature by Sander, Harwood et al. and in the current work are in reasonable agreement when the differing trends in σ(IO) with respect to temperature are taken into account. Confirmation of the negative temperature dependence of the IO cross sections, and hence of k_1, would be provided by a study of the temperature dependence of the IO self-reaction rate coefficient using a different IO detection technique.

The rate coefficient for the IO self-reaction determined in this work at 298 K is in good agreement with recent data evaluations, which have recommended values of 8.0×10^{-11} (ref 3) and 8.9×10^{-11} (ref 14) molecules^{-1} cm^3 s^{-1}. The results of this work suggests that the expression given by DeMore et al.[3] (of $k_1 = 1.5 \times 10^{-11} \exp((500 \pm 500)/T)$ molecules^{-1} cm^3 s^{-1}) overestimates the temperature dependence of k_1: This recommendation was obtained from the mean of the results of Sander[26] and Harwood et al.,[29] while the work reported here is in better agreement with the latter study.

Products, Branching Ratio for the IO Self-Reaction. The experiments performed in the course of this work did not permit direct monitoring of the production of I atoms from the IO self-reaction. The observation of I_2 formation, and its attribution to an IO-catalyzed I atom recombination mechanism, is in keeping with the results reported elsewhere.[28,29] An upper limit of 5% for the branching ratio for the $I_2 + O_2$ channel, i.e., $k_{1b}/k_1 \leq 0.05$ is also consistent with previous studies.[26,28]

OIO has been shown to be a significant product of the IO self-reaction. The wavelength−time coverage afforded by the CCD detection system used in this work facilitated the observation of OIO kinetics. The alternative OIO formation reaction, $IO + O_3$ (reaction 7), may also occur, and a combination of these mechanisms may have been responsible for the OIO observed by Himmelmann et al.[36] in the presence of O_3.

Consideration of the results obtained in the course of this work together with those reported in the literature permits the branching ratio for the IO self-reaction under ambient conditions to be constrained. Previous studies[26,29,30] have shown that production of I atoms accounts for approximately 30% of the IO self-reaction, i.e., $\{(k_{1a} + {}^1/_2 k_{1c})/k_1\} \approx 0.3$ at high (600−760 Torr) pressure. The experiments reported here and in the accompanying paper[43] have determined the branching ratio for the $OIO + I$ product channel of the IO self-reaction to lie in the range $(0.30 \pm 0.05) \leq k_{1c}/k_1 \leq (0.46 \pm 0.08)$. The branching ratio for the atomic channel ($2\,I + O_2$) of the IO self-reaction is therefore constrained: $0.07 \leq k_{1a}/k_1 \leq 0.15$. The production of I_2 from the IO self-reaction has been shown to be negligible ($k_{1b}/k_1 \leq 0.05$) thus the remaining flux through the self-reaction must lead to formation of I_2O_2. The ranges determined for the

branching ratio of the IO self-reaction under ambient conditions (295 ± 3 K; >600 Torr) are therefore

$$IO + IO \rightarrow 2I + O_2 \qquad 0.07-0.15 \qquad (1a)$$

$$\rightarrow I_2 + O_2 \qquad 0-0.05 \qquad (1b)$$

$$\rightarrow OIO + I \qquad 0.30-0.46 \qquad (1c)$$

$$IO + IO + M \rightarrow I_2O_2 + M \qquad 0.42-0.55 \qquad (1d)$$

Determination of the branching ratio for the association channel permits quantification of I_2O_2 formation in the IO self-reaction and hence, assigning absorber P as I_2O_2, derivation of the I_2O_2 absorption cross sections. Only a lower limit can be derived for $\sigma(I_2O_2)$ because the possibility of further reactions consuming I_2O_2 cannot be precluded (as indeed is indicated by the form of the kinetic profile; Figure 13). The maximum branching ratio of $k_{1d}/k_1 = 0.55$ for I_2O_2 formation corresponds to a lower limit for the cross section of $\sigma(I_2O_2) \geq 2.0 \times 10^{-18}$ cm^2 molecule^{-1} at 340 nm.

The negative temperature dependence for the IO + IO reaction indicates that the reaction proceeds through an I_2O_2* association complex. The observation of I_2O_2 as a product of this reaction also indicates that stabilization of the I_2O_2* complex is possible, perhaps in competition with other product channels. The observation of no pressure dependence to k_1 indicates that the contribution of channel 1d to the overall reaction is pressure independent. While this could simply imply that reaction channel 1d is not termolecular or that reaction channel 1d is in its high-pressure limit at all pressures studied in this work, we do not believe this to be the case. The lowest pressure studied in this work was 100 Torr, and the value of k_1 agrees with values obtained from discharge flow studies carried out as low as 2 Torr[32,35] at which the high pressure limit is unlikely to have been reached. An alternative explanation arises from the observation of a pressure dependence to the IO self-reaction in the presence of excess ozone.[26,30] This supports a mechanism in which IO dimer stabilization competes with I atom formation:

$$IO + IO \leftrightarrow I_2O_2^* \rightarrow \text{I atoms}$$
$$\downarrow M$$
$$I_2O_2$$

In this mechanism, the rapid regeneration of IO from I atoms in the presence of excess ozone would lead to an effective suppression of the I atom product channel, and a pressure dependent overall reaction. However, in the absence of ozone, such as in this study no IO regeneration is possible, and no pressure dependence is predicted, as observed. This hypothesis is further supported by the reported high I atom branching ratio $\{(k_{1a} + {}^1/_2k_{1c})/k_1\}$ of 0.65 ± 0.10 from the IO self-reaction at low pressure[35] (2−4 Torr.).

By analogy with the ClO self-reaction, two isomers of I_2O_2 can be envisaged to form directly from the IO self-reaction: IOOI and IOIO. If the IO self-reaction proceeds via an I_2O_2* species which can be collisionally stabilized or may decompose, the high pressure branching ratios reported here, coupled with the high I atom branching ratio reported at low pressures indicates that IOOI* must form to some extent. This conclusion follows the observation that IOOI* would decompose at low pressure to give two iodine atoms, whereas the alternate IOIO* isomer would decompose at low pressure to give a single iodine atom and OIO. The reported branching ratio for iodine atom formation at low pressure therefore cannot be explained from the exclusive formation of IOIO*, and we conclude that IOOI* is the most likely form of the IO association complex. This implies that IOOI is the preferred isomer of stabilized I_2O_2. The formation of IOIO* and thus stabilized IOIO is not precluded: the I atom yield determined merely implies that at least some of the I_2O_2 is IOOI.

Misra and Marshall[54] have conducted computational studies of the IO self-reaction system suggesting that the major products of the IO self-reaction reaction are I + OIO and I_2O_2, with negligible I_2 formation, in agreement with the results of this work. Misra and Marshall also predict the IOIO isomer to be the most stable form of I_2O_2 which could form as a direct product of the IO self-reaction. In the computational studies, the calculated lifetime of IOIO with respect to decomposition to I + OIO was less than 1 ms at 298 K/760 Torr of N_2. This is inconsistent with the identification of I_2O_2 as a stable product of the IO self-reaction in this work, and the total iodine atom yield for the IO self-reaction determined elsewhere.[26,29,30] The experimental studies therefore imply that the I_2O_2 species is more stable than the calculations suggest.

Two previous determinations of lower limits for the cross sections of OIO have been reported in the literature, both (in common with this work) for the most intense peak at approximately 549 nm, at 298 K: Spietz et al.,[42] who determine a lower limit for the cross section of 4×10^{-18} molecules^{-1} cm^2, and estimate the actual value to lie in the range $3-5 \times 10^{-17}$ molecules^{-1} cm^2, and Ingham et al.,[31] who obtain a lower limit to the cross section of 2.7×10^{-17} molecules^{-1} cm^2. These values differ from those obtained in this work (lower limit of 4.15×10^{-18} molecules cm^{-2}; calculated actual range for σ(OIO) of $(0.87-1.29) \times 10^{-17}$ molecules cm^{-2}).

In common with the present study, the cross section lower limit estimates from the literature were obtained by comparing the observed OIO absorption with that calculated on the basis of the known flux through the IO self-reaction, assuming 100% production of OIO + I from IO + IO. Occurrence of any other product channels would reduce the flux through the OIO channel, and lead to the calculated OIO concentrations being overestimated and the OIO cross sections underestimated; hence, the value obtained is a lower limit. However, the reactive loss of OIO, observed in this work (Figure 12) and by Ingham et al., complicates this analysis—the concentration of OIO present at any point in time following photolysis is less than the total amount of OIO generated via IO + IO up to that time, by an amount which is dependent upon the point in time considered. The lower limit to the OIO cross sections determined in the manner described above is thus dependent upon the point in the IO decay/OIO formation at which the calculation is performed, with the smallest values obtained at the shortest times, when the total reactive loss of OIO is least.

If the OIO cross section is calculated immediately following photolysis the cumulative reactive losses of OIO are minimized; this approach will result in the lowest "lower limit" to the cross sections. In this work, the initial gradients of the flux through the IO self-reaction and the OIO absorption with respect to time were compared to obtain the value for $\sigma(OIO)_{min}$ of 4.15×10^{-18} molecules cm^{-2} at $t = 0$. Ingham et al. determined $\sigma(OIO)_{min}$ when 50% of the IO was consumed; were we to adopt this "calculation time" for our data, we would obtain a value of approximately 1.7×10^{-17} molecules cm^{-2} for $\sigma(OIO)_{min}$. The discrepancy between the results of Ingham et al. and the current work may therefore be in part a manifestation of the method used to calculate the lower limit for the OIO cross sections. Spectral resolution may also affect the values of

TABLE 8: Calculated IO Photolysis Rates (s^{-1}), as a Function of SZA and Altitude

SZA	1000 mb	500 mb (≈5.5 km)	75 mb (≈20 km)
40	0.14	0.26	0.27
60	0.10	0.20	0.23
80	0.03	0.09	0.18

$\sigma(OIO)_{min}$ obtained; while this work was performed at 1.13 nm fwhm, Ingham et al. worked at 0.16 nm fwhm and Spietz et al. at 0.22 nm fwhm; thus, lower peak cross sections for a strongly structured absorber such as OIO might be expected under the conditions of this work.

5. Atmospheric Implications

The quantum yield for photolysis of the IO radical has been measured as unity at 355 nm in a recent study by Ingham et al.[31] This value is also is expected to be very close to unity at all other wavelengths of the UV absorption spectrum of IO. The broadband nature of the continuum is indicative of directly dissociative transitions, and while fluorescence has been observed from the (0,0) (2,0) (3,0) and (2,1) bands of the IO ($A^2\Pi \leftarrow X^2\Pi$) transition[55,56] the lifetimes of the states accessed by these transitions is very short (<20 ns)[55] suggesting that they undergo predissociation very rapidly. Recent measurements of the enthalpy of formation of IO[57,58] of 116 ± 5 kJ mol^{-1} correspond to a photolysis threshold of 500 ± 10 nm, i.e. beyond the (0,0) band of the IO ($A \leftarrow X$) transition. A quantum yield of unity for photodissociation of IO was therefore adopted for all absorbing wavelengths in calculation of the IO photolysis rate.

Calculated solar photolysis rates for atmospheric IO as a function of altitude and solar zenith angle (SZA) for 40°N, summer solstice are given in Table 8. The lifetime of the IO radical with respect to photolysis is a few seconds in the sunlit marine boundary layer (MBL). Photolysis rates were calculated using the radiative model of Hough,[59] assuming a total ozone column of 350 Dobson Units. The IO cross sections were averaged and sampled over 5 nm wide integration bins. The IO cross sections reported here exhibit a lower underlying continuum than those measured by Harwood et al.[29] and Laszlo et al.,[26] and give correspondingly reduced IO photolysis rates, by 26% and 34%, respectively. The reduction in IO photolysis rate implies a greater partitioning of IO_x as IO in the atmosphere.

The IO self-reaction has been found to produce I_2O_2 as a major product. The lower limit derived here for the absorption cross sections of I_2O_2 between 340 and 460 nm, corresponds to lower limits to the I_2O_2 photolysis rates of 3.0×10^{-2} and 5.6×10^{-2} s^{-1} for the MBL and the low stratosphere (20 km), respectively (values calculated for noon on the summer solstice at 40°N). The quantum yield for I_2O_2 photodissociation was assumed to be unity throughout the observed spectrum between 340 and 460 nm. If I_2O_2 is indeed IOOI, formation and photolysis of I_2O_2 in the sunlit atmosphere may thus lead to I atom regeneration and catalytic ozone destruction:

$$IO + IO + M \rightarrow IOOI + M \quad (1d)$$

$$IOOI + h\nu \rightarrow IOO + I \quad (32)$$

$$IOO + M \rightarrow I + O_2 + M \quad (33)$$

The mean cross sections calculated for the OIO radical correspond to a photolysis rate of 0.33 s^{-1} in the MBL at noon, 40°N, *if* the quantum yield for OIO photolysis is unity at all wavelengths (495−600 nm). However, recent theoretical calculations[54] suggest that OIO may be photostable, a conclusion supported by recent laboratory studies of the laser photolysis of OIO[31] and by recent atmospheric observations of OIO in the MBL.[60] Because OIO is formed in the IO self-reaction, which will occur to a significant extent at the levels of IO recently observed in the MBL,[15,16] this species may be a significant atmospheric iodine reservoir. This hypothesis is developed in more detail elsewhere.[52] If OIO is indeed photostable, the potential for the IO self-reaction to contribute to ozone depletion will be reduced, as "active" IO_x will be converted to a reservoir form. Moreover, the existence of an additional iodine reservoir species will affect model calculations of the partitioning of inorganic iodine: stratospheric iodine levels will be greater than those inferred previously from IO observations. The potential for iodine chemistry to contribute to stratospheric ozone depletion is considered further in the accompanying paper.[43]

Acknowledgment. We thank Mathew Evans for his help with the photolysis rate calculations, and John Crowley and Jochen Stutz for communication of results prior to publication. W.J.B. thanks the UK NERC for the award of a studentship. D.M.R. thanks the UK NERC for the award of an advanced fellowship. This work was part-funded by the EC Environment program under the project "Laboratory Experiments of Iodine Chemistry in the Stratosphere−LEXIS" (Project number ENV4-CT95-0013)

Supporting Information Available: The wavelength-dependent IO and OIO absorption cross sections determined in the course of this work at 295 K and 1.13 nm fwhm resolution in Tables 4S and 7S, respectively. This material is available free of charge via the Internet at http://pubs.acs.org.

References and Notes

(1) Scientific Assessment of Ozone Depletion: 1998. Report No. 44; World Meterological Organisation Global Ozone Research and Monitoring Project: Geneva, 1999.

(2) Wayne, R. P.; Poulet, G.; Biggs, P.; Burrows, J. P.; Cox, R. A.; Crutzen, P. J.; Hagman, G. D.; Jenkin, M. E.; Le Bras, G.; Moortgat, G. K.; Platt, U.; Schindler, R. N. *Halogen Oxides: Radicals, Sources and Reservoirs in the Laboratory and in the Atmosphere*; Wayne, R. P., Ed.; European Commission: Brussels, 1995. Atmos. Environ. **1995**, *29*, 2675.

(3) DeMore, W. B.; Sander, S. P.; Golden, D. M.; Hampson, R. F.; Kurylo, M. J.; Howard, C. J.; Ravishankara, A. R.; Kolb, C. E.; Molina, M. J. Chemical Kinetics and Photochemical Data for use in Stratospheric Modelling. Evaluation No. 12; JPL Publication 97-4; Jet Propulsion Laboratory: Pasadena, CA, 1997

(4) Chameides, W. L.; Davis, D. D. *J. Geophys. Res.* **1980**, *85*, 7383.

(5) Lovelock, J. E.; Maggs. R. J.; Wade, R. J. *Nature* **1973**, *241*, 194.

(6) Davis, D.; Crawford, J.; Liu, S.; McKeen, S.; Bandy, A.; Thornton, D.; Rowland, F.; Blake, D. *J. Geophys. Res*. **1996**, *101*, 2135.

(7) Oram, D. E.; Penkett, S. A. *Atmos. Environ.* **1994**, *28*, 1159.

(8) Carpenter, L. J.; Sturges, W. T.; Penkett, S. A.; Liss, P. S.; Alicke, B.; Hebestreit, K.; Platt, U. *J. Geophys. Res.* **1999**, *104*, 1679.

(9) Solomon, S.; Garcia. R. R.; Ravishankara, A. R. *J. Geophys. Res.* **1994**, *99*, 20491.

(10) Mössinger, J. C.; Shallcross, D. E.; Cox, R. A. *J. Chem. Soc., Faraday Trans.* **1998**, *94*, 1391.

(11) Rattigan, O. V.; Shallcross, D. E.; Cox, R. A. *J. Chem. Soc., Faraday Trans.* **1997**, *93*, 2839.

(12) Jenkin, M. E. *A* Comparative Assessment of the Role of Iodine Photochemistry in Tropospheric Ozone Depletion. In *The Tropospheric Chemistry of Ozone in the Polar Regions*; Niki, H., Becker, K. H., Eds.; Springer-Verlag: New York, 1993.

(13) Jenkin, M. E.; Cox, R. A.; Mellouki, A.; LeBras, G.; Poulet, G. *J. Phys. Chem.* **1990**, *94*, 2927.

(14) Atkinson, R.; Baulch, D. L.; Cox, R. A.; Hampson, R. F.; Kerr, J. A.; Rossi, M. J.; Troe, J. *EJ. Phys. Chem. Ref. Data* **2000**, *29*, 167.

(15) Alicke, B.; Hebestreit, K.; Stutz, J.; Platt, U. *Nature* **1999**, *397*, 572.

(16) McFiggans, G.; Allan, B. J.; Coe, H.; Plane, J. M. C.; Carpenter, L. J.; O′Dowd, C. D.; Sturges, W. T. *Geophys. Res. Abs*. **1999**, *1*, 520.

(17) Vogt, R.; Sander, R.; VonGlasow, R.; Crutzen, P. J. *J. Atmos. Chem.* **1999**, *32*, 375.

(18) Stutz, J.; Hebstreit, K.; Alicke, B.; Platt, U. *Ann. Geophys. Suppl. 2* **1998**, *16*, C722.
(19) Wennberg, P. O.; Brault, T. F.; Hanisco, R. J.; Salawitch, R. J.; Mount, G. H. *J. Geophys. Res.* **1997**, *102*, 8887.
(20) Pundt, I.; Pommereau, J.-P.; Phillips, C.; Lateltin, E. *J. Atmos. Chem.* **1998**, *30*, 173.
(21) Wittrock, F.; Müller, R.; Richter, A.; Bovensmann, H.; Burrows, J. P. *Geophys. Res. Lett.* **2000**, *27*, 1471.
(22) Durie, R. A.; Ramsay, D. A. *Can. J. Phys.* **1958**, *36*, 35.
(23) Clyne, M. A. A.; Cruse, H. W. *Trans Faraday Soc.* **1970**, *66*, 2227.
(24) Cox, R. A.; Coker, G. B. *J. Phys. Chem.* **1983**, *87*, 4478.
(25) Jenkin, M. E.; Cox, R. A. *J. Phys. Chem.* **1985**, *89*, 192.
(26) Sander, S. P. *J. Phys. Chem.* **1986**, *90*, 2194.
(27) Stickel, R. E.; Hynes, A. J.; Bradshaw, J. D.; Chameides, W. L.; Davis, D. D. *J. Phys. Chem.* **1988**, *92*, 1862.
(28) Laszlo, B.; Kurylo, M. J.; Huie, R. E.; *J. Phys. Chem.* **1995**, *99*, 11701.
(29) Harwood, M. H.; Burkholder, J. B.; Hunter, M.; Fox, R. W.; Ravishankara, A. R. *J. Phys. Chem. A* **1997**, *101*, 853.
(30) Jenkin, M. E.; Cox, R. A.; Candeland, D. E. *J. Atmos. Chem.* **1985**, *2*, 359.
(31) Ingham, T.; Cameron, M.; Crowley, J. N. *J. Phys. Chem. A.* **2000**, *104*, 8001.
(32) Martin, D.; Jourdain, J. L.; Laverdet, G.; LeBras, G. *Int. J. Chem. Kinet.* **1987**, *19*, 503.
(33) Barnes, I.; Bastian, V.; Becker, K. H.; Overath, R. D. *Int. J. Chem. Kinet.* **1991**, *23*, 579.
(34) Atkinson, D. B.; Hudgens, J. W.; Orr-Ewing, A. J. *J. Phys. Chem. A* **1999**, *103*, 6173.
(35) Vipond, A. D. Philos. Thesis, University of Oxford, 1998.
(36) Himmelmann, S. J.; Orphal, J.; Bovensmann, H.; Richter, A.; Ladstätter-Weissenmayer, A.; Burrows, J. P. *Chem. Phys. Lett.* **1996**, *251*, 330.
(37) Nickolaisen, S. L.; Friedl, R. R.; Sander, S. P. *J. Phys. Chem.* **1994**, *98*, 155.
(38) Li, Z. *J. Phys. Chem. A* **1999**, *103*, 1206.
(39) Rattigan, O. V.; Jones, R. L.; Cox, R. A. *Chem. Phys. Lett.* **1994**, *230*, 121.
(40) Rowley, D. M.; Harwood, M. H.; Freshwater, R. A.; Jones, R. L. *J. Phys. Chem.* **1996**, *100*, 3020.
(41) Harwood, M. H.; Rowley, D. M.; Jones, R. L.; Cox, R. A. *J. Phys. Chem. A* **1998**, *102*, 1790.
(42) Spietz, P.; Himmelmann, S.; Gross, U.; Orphal, J.; Burrows, J. P. *Ann. Geophys. Suppl. 2* **1998**, *16*, C722.
(43) Rowley, D. M.; Bloss, W. J.; Cox, R. A.; Jones, R. L. *J. Phys. Chem. A* **2001**, *105*, 7855.
(44) Myer, J. A.; Samsom, J. A. R. *J. Chem. Phys.* **1969**, *52*, 716.
(45) Fahr, A.; Nayak, A. K.; Huie, R. *Chem. Phys.* **1995**, *199*, 275.
(46) Harwood, M. H. Ph.D. Thesis, University of Cambridge, 1995.
(47) Gilles, M. K.; Turnipseed, A. A.; Talukdar, R. K.; Rudich, Y.; Villalta, P. W.; Huey, L. G.; Burkholder, J. B.; Ravishankara, A. R. *J. Phys. Chem.* **1996**, *100*, 14005.
(48) Yuan, J.; Misra, A.; Wells, L.; Hawkins, S.; Krishnan, A.; Nathuji, R. B.; Marshall, P.; Berry, R. Talk J5. Presented at the Fourth International Conference on Chemical Kinetics, Gaithersburg, MD, 1997.
(49) Curtis, A. R.; Sweetenham, W. P. FACSIMILE, AERE. Harwell Publication R 12805; Computer Science and Systems Division, Harwell Laboratory: Oxfordshire, U.K., **1987.**
(50) Calvert, J. G.; Pitts, J. N. *Photochemistry*; John Wiley & Son: New York, 1966.
(51) Bloss; W. J.; Rowley; D. M.; Cox; R. A.; Rowley, D. M. Kinetic Studies of Iodine Oxide Reactions of Atmospheric Importance: 1: The IO + IO Reaction. Presented at the 15th International Symposium on Gas Kinetics, Bilbao, Spain, 1998.
(52) Cox, R. A.; Bloss, W. J.; Jones, R. L.; Rowley, D. M. *Geophys. Res. Lett.* **1999**, *26*, 1857.
(53) Rowley, D. M.; Mossinger, J. C.; Cox, R. A.; Jones, R. L. *J. Atmos. Chem.* **1999**, *34*, 137.
(54) Misra, A.; Marshall, P. *J. Phys. Chem. A* **1998**, *102*, 9056.
(55) Turnipseed, A. A.; Gilles, M. K.; Burkholder, J. B.; Ravishankara, A. R. *Chem. Phys. Lett.* **1995**, *242*, 427.
(56) Hölscher, D.; Zellner, R. Poster PB46. Presented at the 16th International Symposium on Gas Kinetics, Cambridge, U.K., July 2000.
(57) Bedjanian, Y.; LeBras, G.; Poulet, G. *J. Phys. Chem. A* **1997**, *101*, 4088.
(58) Gilles, M. K.; Turnipseed, A. A.; Burkholder, J. B.; Ravishankara, A. R. *Chem. Phys. Lett.* **1997**, *272*, 75.
(59) Hough, A. M. UK AEA Report R13259; Computer Science and Systems Division, Harwell Laboratory: Oxfordshire, U.K., **1988.**
(60) Stutz, J.; Hebestreit, K.; Hoenninger, G.; Platt, U. *Geophys. Res. Abs.* **1999**, *1*, 520.